The aggregation of an alky-C$_{60}$ derivative as a function of concentration, temperature and solvent type

Supporting Information

Martin J. Hollamby,*[a] Catherine Smith,[b] Melanie Britten,[b] Ashleigh Danks,[b] Zoe Schnepp,[b] Isabelle Grillo,[c] Brian R. Pauw,[d] Akihiro Kishimura,[e] and Takashi Nakanishi[f]

[a] *School of Physical and Geographical Sciences, Keele University, Keele, Staffordshire, ST55BG, UK; Tel: +44 1782 733532; E-mail: m.hollamby@keele.ac.uk*

[b] *School of Chemistry, University of Birmingham, B15 2TT, UK*

[c] *Institut Max-von-Laue-Paul-Langevin, BP 156-X, F-38042 Grenoble, Cedex, France*

[d] *BAM Federal Institute for Materials Research and Testing, Unter den Eichen 87, 12205 Berlin, Germany*

[e] *Department of Chemistry and Biotechnology, Graduate School of Engineering, The University of Tokyo, Japan*

[f] International Center for Materials Nanoarchitechtonics, National Institute for Materials Science, 1-2-1 Sengen, Tsukuba 305-0047, Japan

SANS & SAXS data fitting

Mixed model

Unless otherwise noted, the following equations have been taken from the SASfit[1] documentation and used directly, with only minor modification to parameter signifiers.

As explained in the MS, a mixed model comprising a summed combination of a Schultz distribution of (i) polydisperse core-shell spheres[2,3] and (ii) a Lorentzian peak function was used to model the contributions arising from (i) micelle-like clusters and (ii) the developing network, respectively. Other approaches using different micelle shapes and more complicated models, for example taking into account the probable existence of associated monomers in all samples, were trialled extensively. However this model was chosen as it is relatively simple and can been applied to all datasets with great success (as shown). The possibility that the emerging peak could be accounted for by a hard sphere structure factor[4] was considered, but disregarded as incorporating it led to poor agreement with the data. This is because the peak is poorly apparent in the perdeuterated data and non-existent in the CM-C_{60} data, while the secondary oscillations present in the hard sphere S(Q) model were not observed in the CM-alkyl data.

The form factor, P(Q) for the micelles were modelled as a Schulz distribution of spherical core-shell particles. The general equation for $K(Q,r,\Delta\rho)$ of a solid sphere, where r is the radius and $\Delta\rho$ is the contrast step, is as follows:

$$K(Q,r,\Delta\rho) = \frac{4}{3}\pi r^3 \Delta\rho\, 3\frac{sinQr - QrcosQr}{(Qr)^3}$$

For core-shell particles, the overall $I(Q)_{mic}$ is described below, in which r_{core} is the core radius, δ_{shell} the shell thickness, and $\Delta\rho_{solv-core}$, $\Delta\rho_{solv-shell}$ are the scattering contrasts relative to the solvent for the core and shell respectively:

$$I\big(Q,r_{core},\delta_{shell},\Delta\rho_{solv-core},\Delta\rho_{solv-shell}\big)_{mic}$$
$$= N\big[K\big(Q,r_{core} + \delta_{shell},\Delta\rho_{solv-shell}\big) - K\big(Q,r_{core},\Delta\rho_{solv-shell} - \Delta\rho_{solv-core}\big)\big]^2$$

where N is the scale factor that is related to the number density of scatterers per unit volume. The Schulz distribution,[2] commonly used for self-associating surfactant micelles and microemulsion droplets,[3] is given as follows:

$$Schulz(r,\bar{r},Z) = \left(\frac{Z+1}{\bar{r}}\right)^{Z+1} \left(\frac{r^Z \exp\left[\dfrac{-r(Z+1)}{r}\right]}{\Gamma(Z+1)}\right)$$

Here, r is the distributed radius (which was r_{core}), $\bar{r}$ is the mean of the distribution and Z is the width parameter, from which the dispersity σ is calculated as:

$$\sigma = \frac{\bar{r}}{(Z+1)^{1/2}}$$

Finally, the Lorentzian peak function, scaled by the amplitude A, is given as follows:

$$I(Q,Q_{peak},w_{peak},A)_{peak} = \frac{A}{\pi}\left[\frac{w_{peak}}{(Q - Q_{peak})^2 + w_{peak}{}^2}\right]$$

Here, Q_{peak} is the peak position and w_{peak} is the half width at half maximum. The total scattering for each sample was calculated as the sum of contributions from the peak, core-shell micelles and flat incoherent background, I_{bkg} as follows:

$$I(Q) = I(Q)_{mic} + I(Q)_{peak} + I_{bkg}$$

OZ + peak model

The SAXS data was also analysed using the following model, which has previously been applied to bicontinuous emulsions.

$$I(Q)_{OZ + peak} = \frac{I_0}{1 + Q^2\xi^2} + \frac{A_{peak,OZ}}{\pi}\left[\frac{w_{peak,OZ}}{(Q - Q_{peak,OZ})^2 + w_{peak,OZ}{}^2}\right] + I_{bkg,OZ}$$

Here, I_0 is the forward scattering at $Q = 0$, ξ is the correlation length, $A_{peak,OZ}$ is the peak amplitude, $Q_{peak,OZ}$ is the peak position, $w_{peak,OZ}$ is the half width at half maximum and $I_{bkg,OZ}$ is the flat background contribution.

Teubner-Strey model

The SAXS data was also modelled using the Teubner-Strey model, which has also been previously applied to bicontinuous systems.

$$I(Q)_{TS} = \frac{8\pi\langle\eta^2\rangle}{\xi_{TS}(a^2 - 2bQ^2 + Q^4)} + I_{bkg,TS}$$

Where $a^2 = (k^2 + 1/\xi_{TS}^2)$, $b = k^2 + 1/\xi_{TS}^2$ and $k = 2\pi/d_{TS}$. The parameter $\langle\eta^2\rangle$ is mean square scattering length density fluctuation, which is related to the volume fraction of the two phases and the scattering contrast step between them. The domain size, d_{TS} represents a quasi-periodic repeat distance between C_{60} and alkyl regions within the solution, while the correlation length, ξ_{TS} corresponds to a characteristic length for positional correlation.

Density and scattering length density estimation

Contrast-variation SANS experiments used fully deuterated solvents or mixtures of deuterated and hydrogentated solvent. In using mixtures, the aim was to match the scattering length density, ρ of the solvent to that of C_{60} or of the alkyl parts of **1** respectively. Taking the solvent n-hexane as an example, n-hexane-h_{14} has $\rho = -0.57 \times 10^{-6}$ Å^{-2}, while n-hexane-d14 has $\rho_d = 6.14 \times 10^{-6}$ Å^{-2}. Given that n-hexane-h_{14} and n-hexane-d_{14} are fully miscible, mixing the solvents together gives a tuneable solvent ρ in the range -0.57 to 6.14×10^{-6} Å^{-2}. Therefore the relative amounts of n-hexane-h_{14} and n-hexane-d_{14} required in each case can be calculated, provided the scattering length density of the C_{60}, ρ_{C60} and alkyl, ρ_{alkyl} parts of **1** is known.

The alkyl part of **1**, *i.e.* the whole molecule minus C_{60}, was estimated to have a density of 0.9 g mL^{-1} using the in-built calculator in ACD/ChemSketch. This results in $\boldsymbol{\rho_{alkyl} = 1 \times 10^{-7}}$ Å^{-2}, found using the NIST Neutron scattering calculator, at https://www.ncnr.nist.gov/resources/activation/.

An estimate for ρ_{C60} in the studied system might be found by considering ρ_{C60} of pure cyrstalline C_{60}. This has a density that depends on the crystal structure, but that is typically around 1.7 g cm^{-3}.[5] On this basis, $\rho_{C60} = 5.7 \times 10^{-6}$ Å^{-2}. However, in the less ordered state inside a micelle, the density and therefore ρ_{C60} is likely to be lower than this. This same issue was noted and accounted for

previously by Yin and Dadmun[6] who used 3.6×10^{-6} Å^{-2} for amorphous regions of [6,6]-phenyl-C_{61}-butyric acid methyl ester (PCBM) instead of the predicted value of 5.0×10^{-6} Å^{-2} based on its crystalline density.

Previously, the van der Waals volume, which can be fairly accurately estimated from the molecular composition and geometry, multiplied by a factor of 1.6 has been used to predict the molar volume of polymers, from which the density can be calculated for a molecule of known molecular weight.[7] Literature value for the van der Waals volume of C_{60} range from $450 - 550$ Å^3 molecule^{-1} ($271 - 331$ cm^3 mol^{-1}).[8] If 331 cm^3 mol^{-1} is used with the same multiplication factor (1.6), the molar volume of C_{60} is predicted to be 540 cm^3 mol^{-1}, giving a bulk density of 1.33 g cm^{-3} and $\rho_{C60} = 4.4 \times 10^{-6}$ Å^{-2}. However, in reality, even in a disordered state the interactions between compact C_{60} units will be stronger[9] than the interactions between polymer chains, which would increase the density (and ρ_{C60}).

Using these high and low estimations, it is therefore likely that in **1** the theoretical density of the C_{60} unit should lie between 1.33 and 1.7 g mL^{-1} and consequently ρ_{C60} should lie between 4.4 and 5.7 $\times 10^{-6}$ Å^{-2}. The midpoint of these ranges is **density = 1.5 g mL^{-1}** and ρ_{C60} = **5 $\times$ 10^{-6} Å^{-2}**, whcih are the values use in this work. This estimate of ρ_{C60} is lower than those suggested by others (*e.g.* 5.6 $\times$ 10^{-6} Å^{-2} or 7.6 $\times$ 10^{-6} Å^{-2}),[10,11] but judging from the SANS data it is close to reality, as the separation of scattering from core and shell was achieved. Using this approximation, the effective volume occupied by C_{60} in the micelle is therefore 780 Å^3 molecule^{-1}.

To estimate the density of **1** that was used to calculate the concentration of all samples and to calculate the volume fractions for the diffusion NMR data, a linear combination of the estimated densities of the alkyl and C_{60} parts, scaled by molecular weight, was used, as follows:

$$density = 0.9 \times \frac{863}{1559} + 1.5 \times \frac{720}{1559} = 1.17 \text{ g mL}^{-1}$$
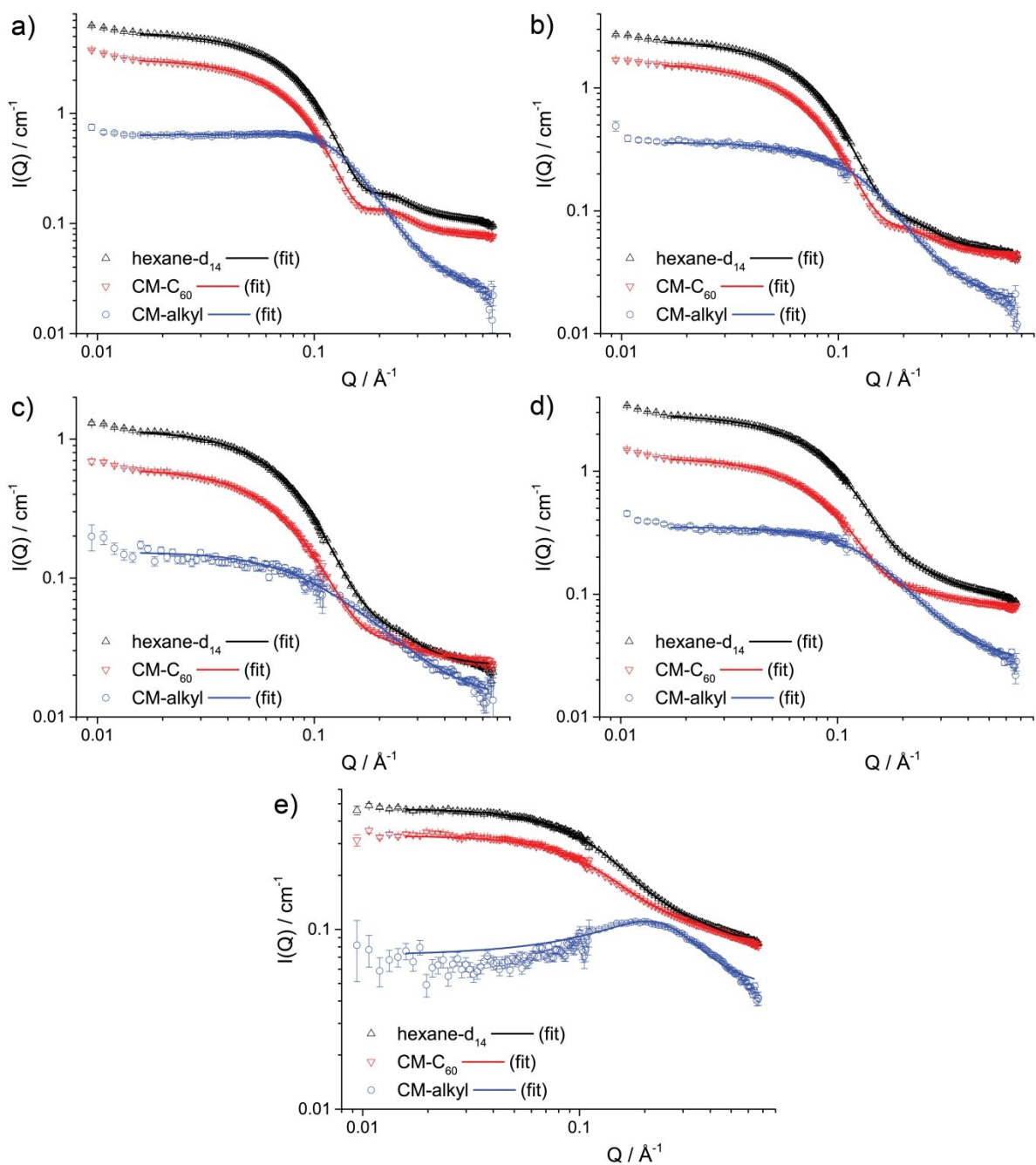
Figure S1. CV-SANS data for (a) 0.1 M **1** in *n*-hexane at 10 °C, (b) 0.05 M **1** in *n*-hexane at 25 °C, (c) 0.025 M **1** in *n*-hexane at 25 °C, (d) 0.1 M **1** in *n*-decane at 25 °C, and (e) 0.1 M **1** in toluene at 25 °C, showing the three contrast profiles highlighting the scattering contributions from the micelle core (CM-alkyl), shell (CM-C_{60}) and whole micelle (either hexane-d_{14}, decane-d_{22} or toluene-d_8), as described in the MS text. In all panels, solid lines are fits to the data, using a model combining contributions from (i) a Schulz distribution of core-shell spheres, (ii) a Lorentzian peak function and (iii) a flat background.
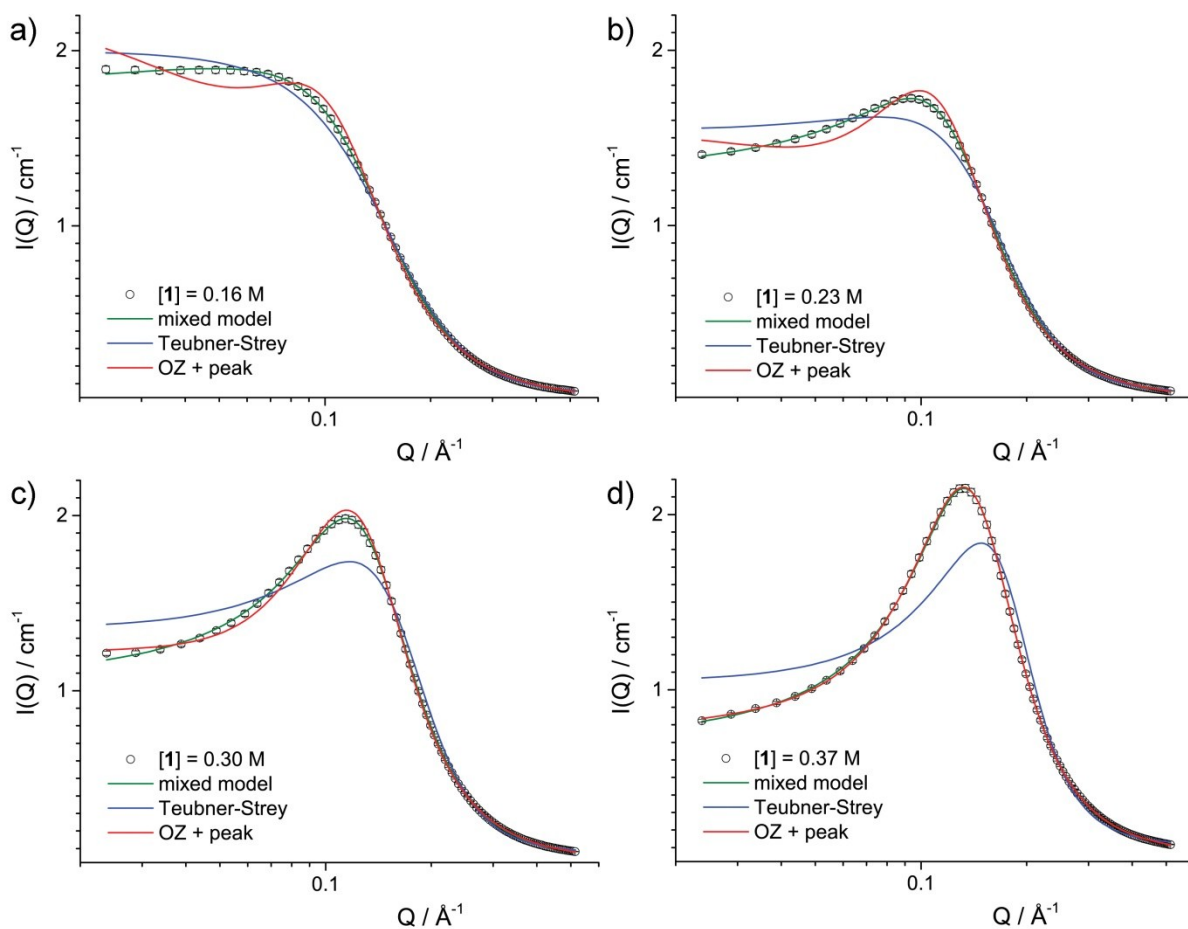
Figure S2. Comparison of models used to fit the SAXS data for samples of **1** in *n*-decane at 25 °C, with [**1**] ranging from 0.16 to 0.37 M. Fitted parameters for the OZ + peak (OZ) and Teubner-Strey (TS) models are provided in Table S3 and S4, while those for the mixed model are shown in Tables 1 and S2. The mixed model provides the closest agreement with data in all cases, although the OZ model shows equally good agreement at [**1**] = 0.37 M. Interestingly, both the mixed and OZ models show the same trends, with a general decrease in domain size (via r_{core} or ξ_{OZ}) as the concentration increases. Moreover, peak parameters across the concentration range are very comparable. The Teubner-Strey approach shows an increase in correlation length ξ_{TS} with concentration, but a decrease in domain size. Using this model, a transition from $d_{TS} / 2\pi\xi_{TS} > 1$ to $d_{TS} / 2\pi\xi_{TS} < 1$ as seen between [**1**] = 0.16 and 0.23 M is often ascribed to a system change from mainly clustered to mainly bicontinuous. While this would support the emergence of a bicontinuous network, this transition cannot have too much weight assigned to it due to the poor agreement of the TS model with the data.
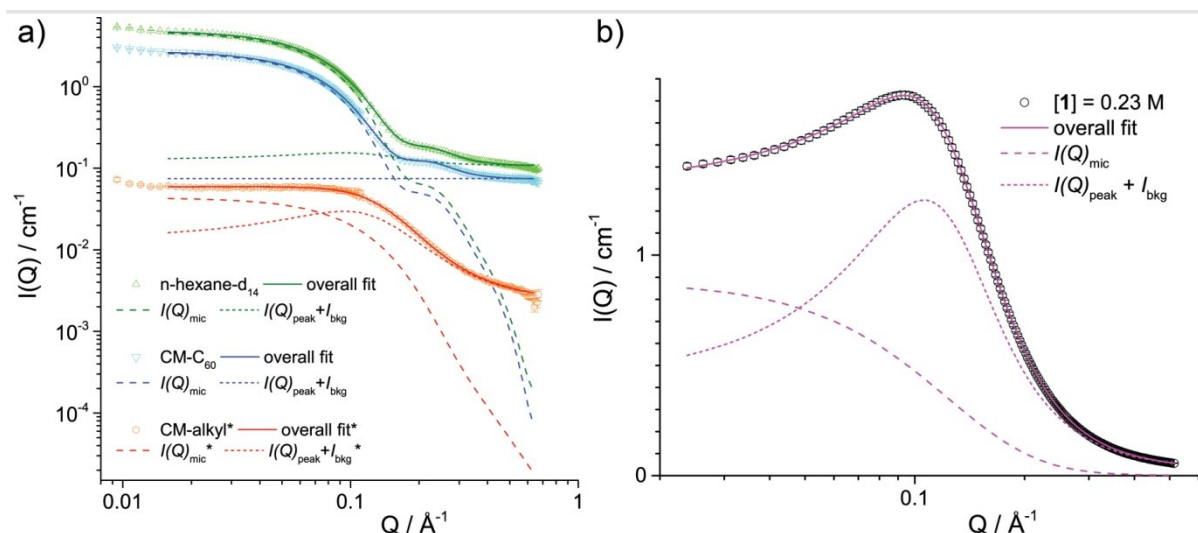
Figure S3. Breakdown of the contributions to the overall fit from the micelle population, $I(Q)_{mic}$, the peak function $I(Q)_{peak}$ arising from spacial separation between domains within the growing network and the flat background I_{bkg} for (a) 0.1 M **1** in *n*-hexane (SANS data) and (b) 0.23 M **1** in *n*-decane (SAXS data), both at 25 °C. *In panel (a), the CM-alkyl data and according fits have all been divided by a factor of 10 for clarity.
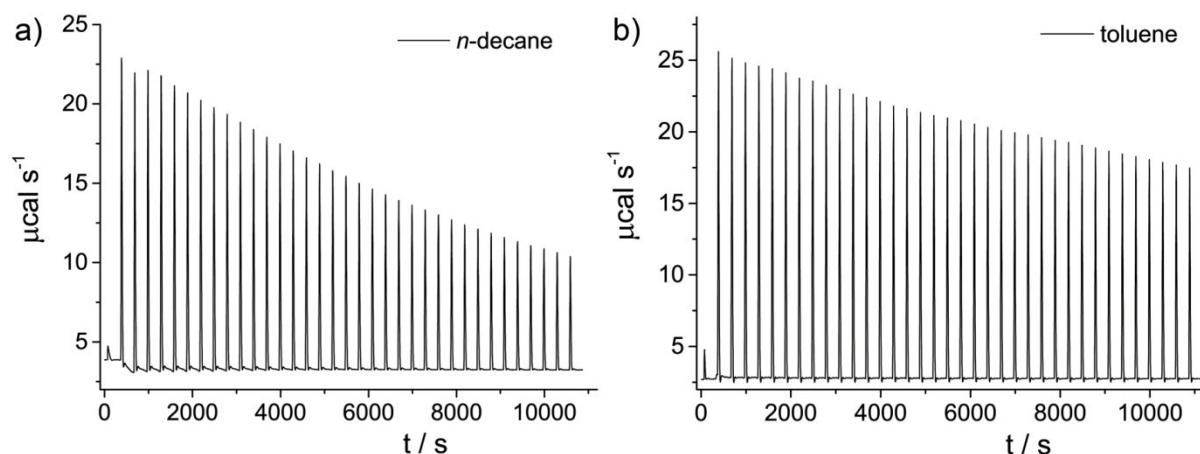

Figure S4. Raw data, prior to background subtraction, of recorded calorimetric response from repeated injections of a concentrated solution of **1** in (a) *n*-decane ([**1**] = 124 mM) into pure *n*-decane and (b) toluene ([**1**] = 124 mM) into pure toluene. In both cases, after an initial injection (1 μL), each peak indicates a single injection of 8 μL.

Table S1: Additional fitted parameters that were not shown in Table 1, and calculated values for solvent penetration into the alkyl region/shell of **1**, from analysis of the SANS data shown in Fig 1b and Fig S1.

[1] / M	T / °C	Solvent	N	ρ_{shell}/ Å^{-2} (100% D)	% solvent in shell (100% D)	ρ_{shell}/Å^{-2} (CM C$_{60}$)	% solvent in shell (CM C$_{60}$)	A_{peak} / cm^{-1} (100% D)	I_{bkg} / cm^{-1} (100% D)	I_{bkg} / cm^{-1} (CM C$_{60}$)	I_{bkg} / cm^{-1} (CM alkyl)
0.1	10	*n*-hexane	127.7	1.58 × 10^{-6}	25	1.40 × 10^{-6}	27	0.033	0.108	0.079	0.020
0.1	25	*n*-hexane	110.0	1.46 × 10^{-6}	23	1.33 × 10^{-6}	25	0.048	0.108	0.075	0.024
0.05	25	*n*-hexane	54.5	1.62 × 10^{-6}	25	1.20 × 10^{-6}	22	0.026	0.047	0.045	0.017
0.025	25	*n*-hexane	33.0	1.71 × 10^{-6}	27	1.68 × 10^{-6}	32	0.016	0.023	0.027	0.013
0.1	25	*n*-decane	133.7	1.35 × 10^{-6}	19	1.28 × 10^{-6}	24	0.105	0.091	0.084	0.026
0.1	25	toluene	88.2	0.81 × 10^{-6}	13	1.18 × 10^{-6}	22	0.049	0.083	0.084	0.046

Table S2: Additional fitted parameters that were not shown in Table 1 from analysis of the SAXS data measured in *n*-decane and at 25 °C shown in Fig 1c.

[1] / M	N	I_{bkg} / cm^{-1}
0.16	593.3	0.020
0.23	633.2	0.020
0.30	1105.3	0.039
0.37	1632.4	0.061

Table S3. Fitted parameters from analysis of the SAXS data measured in *n*-decane and at 25 °C shown in Fig 1c and Fig S2, using the OZ + peak model explained above.

[1] / M	$I_{0,OZ}$	ξ_{OZ} / Å	$A_{peak,OZ}$ / cm^{-1}	$Q_{peak,OZ}$ / Å^{-1}	$w_{peak,OZ}$ / Å^{-1}	$I_{bkg,OZ}$ / cm^{-1}
0.16	1.654	21.3	1.43	0.093	0.066	0.0068
0.23	1.061	19.1	1.54	0.104	0.064	0.0069
0.30	0.715	16.8	1.86	0.117	0.064	0.0242
0.37	0.270	15.1	2.05	0.132	0.065	0.0524

Table S4. Fitted parameters, and calculated values for d_{TS} / $2\pi\xi_{TS}$ from analysis of the SAXS data measured in *n*-decane and at 25 °C shown in Fig 1c and Fig S2, using the Teubner-Strey model explained above.

[1] / M	$<\eta^2>_{TS}$	ξ_{TS} / Å	d_{TS} / Å	d_{TS} / $2\pi\xi_{TS}$	$I_{bkg,TS}$ / cm^{-1}
0.16	0.0200	8.5	60.9	1.14	0.0446
0.23	0.0200	10.0	49.9	0.80	0.0465
0.30	0.0219	11.6	43.3	0.59	0.0753
0.37	0.0232	13.8	38.1	0.44	0.116

Supporting references

1 I. Breßler, J. Kohlbrecher and A. F. Thünemann, SASfit : a tool for small-angle scattering data analysis using a library of analytical expressions, *J. Appl. Cryst.*, 2015, **48**, 1587–1598.

2 G. V. Z. Schulz, *Phys. Chem.*, 1939, **B43**, 25.

3 M. Kotlarchyk, R. B. Stephens and J. S. Huang, Study of Schultz distribution to model polydispersity of microemulsion droplets, *J. Phys. Chem.*, 1988, **92**, 1533–1538.

4 A. Vrij, Mixtures of hard spheres in the Percus-Yevick approximation. Light scattering at finite angles, *J. Chem. Phys.*, 1979, **71**, 3267–3270.

5 Y. Quo, N. Karasawa and W. A. Goddard, Prediction of fullerene packing in C_{60} and C_{70} crystals, *Nature*, 1991, **351**, 464–467.

6 W. Yin and M. Dadmun, A New Model for the Morphology of P3HT/PCBM Organic Photovoltaics from Small-Angle Neutron Scattering: Rivers and Streams, *ACS Nano*, 2011, **5**, 4756–4768.

7 D. W. Van Krevelen and P. J. Hoftyzer, Prediction of polymer densities, *J. Appl. Polym. Sci.*, 1969, **13**, 871–881.

8 G. B. Adams, M. O'Keeffe and R. S. Ruoff, Van Der Waals Surface Areas and Volumes of Fullerenes, *J. Phys. Chem.*, 1994, **98**, 9465–9469.

9 A. Sygula and S. Saebø, π-π Stacking of curved carbon networks: The corannulene dimer, *Int. J. Quantum Chem.*, 2009, **109**, 65–72.

10 V. L. Aksenov, M. V. Avdeev, T. V. Tropin, M. V. Korobov, N. V. Kozhemyakina, N. V. Avramenko and L. Rosta, Formation of fullerene clusters in the system C_{60}/NMP/water by SANS, *Phys. B Condens. Matter*, 2006, **385–386**, 795–797.

11 U. Jeng, T.-L. Lin, W.-J. Liu, C.-S. Tsao, T. Canteenwala, L. Y. Chiang, L. P. Sung and C. C. Han, SANS and SAXS study on aqueous mixtures of fullerene-based star ionomers and sodium dodecyl sulfate, *Phys. A*, 2002, **304**, 191–201.